INTERNATIONAL JOURNAL FOR NUMERICAL METHODS IN FLUIDS
Int. J. Numer. Meth. Fluids 2005; **49**:1147–1167
Published online 3 August 2005 in Wiley InterScience (www.interscience.wiley.com). DOI: 10.1002/fld.1043

Excitation of shear layer instability in flow past a cylinder at low Reynolds number

S. Mittal*,†

Department of Aerospace Engineering, Indian Institute of Technology Kanpur, Kanpur, UP 208 016, India

SUMMARY

The instability of the separated shear layer for flow past a cylinder, in two dimensions, is investigated for low Reynolds numbers ($Re \leqslant 350$). The line of symmetry, downstream of the cylinder, in the wake is forced to be a streamline. This hypothetical situation allows slip of velocity along the wake centreline but prevents any flow normal to it. With this arrangement the flow is completely stable for $Re \leqslant 250$. It suppresses the primary instability of the wake that is responsible for the von Karman vortex shedding. Unlike the conventional splitter plate such an arrangement does not have a wake of its own. At $Re = 300$ and above the wake instability and the shear layer instability are observed. The fluctuations due to the instabilities are intermittent in nature. The shear layer frequency is smaller than the frequency of the von Karman vortex shedding for the regular flow past a cylinder. It is also found that flow past half a cylinder, with symmetry conditions at the wake centreline, at $Re = 300$ is stable. However, when a secondary cylinder with one-fifth the diameter of the half-cylinder is placed close to it, the vortex shedding from the smaller cylinder again leads to instability of the separated shear layer of the half-cylinder. This suggests that although the separated shear layer is stable, at such low *Re*, the shear layer instability can be excited by some other disturbances. It is found that even at such low *Re*, the normalized shear layer frequency follows the $Re^{0.67}$ power law. All the computations have been carried out using a stabilized finite element formulation. Copyright © 2005 John Wiley & Sons, Ltd.

KEY WORDS: vortex shedding; cylinder; wake bubble; suppression; secondary cylinder; shear layer instability

1. INTRODUCTION

The flow past a cylinder is associated with various instabilities [1, 2]. At $Re \sim 47$ the primary instability of the wake results in von Karman vortex shedding. The flow remains

*Correspondence to: Sanjay Mittal, Department of Aerospace Engineering, Indian Institute of Technology Kanpur, Kanpur, UP 208 016, India.
†E-mail: smittal@iitk.ac.in

Contract/grant sponsor: Department of Science and Technology, India

Received 1 November 2004
Revised 6 April 2005
Accepted 24 April 2005

two-dimensional at low Re while three-dimensional transitions in the wake are observed at Re larger than, approximately, 190 [1]. Instability of the separated shear layer due to the Kelvin–Helmholtz mechanism is observed at higher Re. Various values of the critical Reynolds number (Re_c), at which this instability is first observed, have been reported in the literature. Gerrard [3] observed the shear layer instability at $Re = 350$ and higher. Prasad and Williamson [4] found that the end-conditions determine the Re_c; it is $\sim$1200 for parallel shedding conditions and significantly higher ($\sim$2600) for the end-conditions that result in oblique shedding. Unal and Rockwell [5] have reported that they are unable to observe shear layer transition waves for $Re < 1900$ using flow visualization. Bloor [6] observed the shear layer instability for Re larger than 1300. The observation of the transition waves for $Re \sim 350$ by Gerrard [3] remains unexplained to this date.

It was observed by Prasad and Williamson [4] that the shear layer fluctuations are intermittent and become stronger with increase in Re. They also presented an explanation for the intermittent behaviour of these fluctuations. The cause is the the streamwise movement of the point in the shear layer at which the fluctuations develop rapidly. Williamson [1] has presented an explanation as to why the shear layer vortices are not observed for $Re < 1200$.

The present work is an effort to investigate the possibility of observing the shear layer fluctuations at low Re. At low Re, the shear layer transition waves are very weak and the flow is dominated by the primary instability of the wake. A computational experiment is designed that results in suppression/weakening of the primary wake instability but does not annihilate the instability of the separated shear layer(s). This may allow one to observe the shear layer vortices even at low Re. It was shown by us in an earlier work [7] that a 'slip' splitter plate occupying a certain portion of the centreline downstream of the cylinder results in complete suppression of vortex shedding for low Re. The component of velocity normal to the 'slip' plate is zero but that along the plate remains unaltered. For $Re = 100$ flow a slip plate of length $2D$ (D is the diameter of the cylinder) whose leading edge is located at $2.68D$ from the centre of the cylinder is sufficient to completely suppress the vortex shedding. The location and length of the slip plate required to suppress the shedding is a function of the Reynolds number.

In the present work, computations are carried out for flow past a cylinder at low Reynolds numbers ($50 \leqslant Re \leqslant 350$). First, the steady-state solutions and the fully developed unsteady solutions, following an impulsive start, are computed. These results are compared with those available in the literature. Computations are also carried out for the case where the centreline, in the wake downstream of the cylinder, is forced to be a streamline. In this scenario the flow for $Re = 250$ and lower remains stable. However, the flow at $Re = 300$ becomes unstable. Both, the primary instability of the wake and the instability of the separated shear layer are observed. It is well known that the $Re = 300$ flow past a cylinder is associated with three-dimensional instabilities. However, the objective of the present work is to study the instability of the separated shear layer. This instability, along the span of the cylinder, is by and large two-dimensional [1, 8]. Results are also presented for the $Re = 350$ flow. The data from the simulations for $Re = 300$ and 350 is utilized to see if the normalized shear layer frequency follows the power law, $Re^{0.67}$, as shown by Prasad and Williamson [4] for higher Re flows.

While a conventional splitter plate interferes with the flow even for the unperturbed basic flow, forcing the centreline to be a streamline does not alter the basic steady-state flow. The steady-state flows for the two cases, with and without forcing the centreline to be a streamline, are identical. The effect of a conventional splitter plate has been investigated by

other researchers in the past. Roshko [9] observed that a splitter plate of chord $5D$ results in suppression of shedding. A plate of chord $1D$ does not inhibit formation of vortices but changes the shedding frequency slightly. Unal and Rockwell [5, 10] carried out a similar study. They found that by placing the plate appropriately, compared to a cylinder with no control, it is possible to more than double the vortex formation length. For low Re the vortex shedding is completely eliminated while for higher Re the large-scale shedding is suppressed but the shear layer instability remains.

To investigate further the excitation of shear layer instability by external disturbances, the effect of placing a secondary cylinder close to the separated shear layer from half a cylinder is studied for $Re = 300$. The diameter of the secondary cylinder is one-fifth that of half the cylinder. Still, the effective Re for the smaller cylinder is large enough to result in a von Karman vortex street. This interacts with the shear layer from the half-cylinder and results in shear layer instability.

The outline of the rest of the article is as follows. We begin by reviewing the governing equations for incompressible fluid flow in Section 2. Section 3 describes the stabilized finite element formulation. The problem set-up is described in Section 4, while the computational results are presented in Section 5. First, to establish confidence in the computational methods and the results, comparisons with published data is presented. Later, results that point to the presence of shear layer instability are shown. We close with some concluding remarks made in Section 6.

2. THE GOVERNING EQUATIONS

Let $\Omega \subset \mathbb{R}^{n_{\text{sd}}}$ and $(0, T)$ be the spatial and temporal domains, respectively, where n_{sd} is the number of space dimensions, and let Γ denote the boundary of Ω. The spatial and temporal coordinates are denoted by $\mathbf{x}$ and t. The Navier–Stokes equations governing incompressible fluid flow are

$$\rho\left(\frac{\partial \mathbf{u}}{\partial t} + \mathbf{u}\cdot\nabla\mathbf{u} - \mathbf{f}\right) - \nabla\cdot\boldsymbol{\sigma} = 0 \quad \text{on } \Omega \text{ for } (0,T) \tag{1}$$

$$\nabla\cdot\mathbf{u} = 0 \quad \text{on } \Omega \text{ for } (0,T) \tag{2}$$

Here ρ, $\mathbf{u}$, $\mathbf{f}$ and $\boldsymbol{\sigma}$ are the density, velocity, body force and the stress tensor, respectively. The stress tensor is written as the sum of its isotropic and deviatoric parts:

$$\boldsymbol{\sigma} = -p\mathbf{I} + \mathbf{T}, \quad \mathbf{T} = 2\mu\boldsymbol{\varepsilon}(\mathbf{u}), \quad \boldsymbol{\varepsilon}(\mathbf{u}) = \tfrac{1}{2}((\nabla\mathbf{u}) + (\nabla\mathbf{u})^{\mathrm{T}}) \tag{3}$$

where p and μ are the pressure and coefficient of dynamic viscosity. These equations are accompanied with appropriate boundary conditions and an initial condition. The internal as well as the external boundary of the domain, Γ, is partioned in Γ_g and Γ_h. In general, the boundary conditions are either on the velocity field ($\mathbf{u} = \mathbf{g}$ on Γ_g) or on the stress ($\mathsf{n}\cdot\boldsymbol{\sigma} = \mathbf{h}$ on Γ_h). For the flow problem being studied in this paper they are described in more detail in Section 4.

3. FINITE ELEMENT FORMULATION

The incompressible flow equations, in the velocity pressure form, are solved via a stabilized finite element method. The stabilized formulation is based on the streamline-upwind/Petrov–Galerkin (SUPG) and pressure-stabilizing/Petrov–Galerkin (PSPG) stabilization techniques. Several element-level integrals are added to the Galerkin formulation to stabilize the computations against spurious numerical oscillations. The basic Galerkin formulation is unstable for large *Re* flows and does not allow one to use equal-order-interpolation velocity–pressure elements. The time integration of the governing flow equations is done via an implicit procedure that is second-order accurate. The time steps are chosen to adequately resolve the time-scales in the physical phenomena. The large-scale-coupled nonlinear equation systems resulting from the finite element discretization of the governing equations are solved iteratively by employing the Generalized Minimal RESidual (GMRES) procedure in conjunction with diagonal preconditioners.

Consider a finite element discretization of Ω into subdomains Ω^e, $e=1,2,\ldots,n_{\text{el}}$, where n_{el} is the number of elements. Based on this discretization, for velocity and pressure we define the finite element trial function spaces $\mathscr{S}_{\mathbf{u}}^h$ and $\mathscr{S}_p^h$, and weighting function spaces $\mathscr{V}_{\mathbf{u}}^h$ and $\mathscr{V}_p^h$. These function spaces are selected, by taking the Dirichlet boundary conditions into account, as subsets of $[\mathbf{H}^{1h}(\Omega)]^{n_{\text{sd}}}$ and $\mathbf{H}^{1h}(\Omega)$, where $\mathbf{H}^{1h}(\Omega)$ is the finite-dimensional function space over Ω. The stabilized finite element formulation of Equations (1)–(2) is written as follows: find $\mathbf{u}^h \in \mathscr{S}_{\mathbf{u}}^h$ and $p^h \in \mathscr{S}_p^h$ such that $\forall \mathbf{w}^h \in \mathscr{V}_{\mathbf{u}}^h$, $q^h \in \mathscr{V}_p^h$

$$\begin{aligned}
&\int_\Omega \mathbf{w}^h \cdot \rho\left(\frac{\partial \mathbf{u}^h}{\partial t} + \mathbf{u}^h \cdot \boldsymbol{\nabla}\mathbf{u}^h - \mathbf{f}\right) \mathrm{d}\Omega + \int_\Omega \boldsymbol{\varepsilon}(\mathbf{w}^h) : \boldsymbol{\sigma}(p^h, \mathbf{u}^h)\, \mathrm{d}\Omega + \int_\Omega q^h \boldsymbol{\nabla}\cdot\mathbf{u}^h \, \mathrm{d}\Omega \\
&\quad + \sum_{e=1}^{n_{\text{el}}} \int_{\Omega^e} \frac{1}{\rho}(\tau_{\text{SUPG}}\rho\mathbf{u}^h \cdot \boldsymbol{\nabla}\mathbf{w}^h + \tau_{\text{PSPG}}\boldsymbol{\nabla} q^h) \\
&\quad \cdot \left[\rho\left(\frac{\partial \mathbf{u}^h}{\partial t} + \mathbf{u}^h \cdot \boldsymbol{\nabla}\mathbf{u}^h - \mathbf{f}\right) - \boldsymbol{\nabla}\cdot\boldsymbol{\sigma}(p^h, \mathbf{u}^h)\right] \mathrm{d}\Omega^e \\
&\quad + \sum_{e=1}^{n_{\text{el}}} \int_{\Omega^e} \tau_{\text{LSIC}} \boldsymbol{\nabla}\cdot\mathbf{w}^h \rho \boldsymbol{\nabla}\cdot\mathbf{u}^h \, \mathrm{d}\Omega^e = \int_{\Gamma_h} \mathbf{w}^h \cdot \mathbf{h}^h \, \mathrm{d}\Gamma
\end{aligned} \tag{4}$$

In the variational formulation given by Equation (4), the first three terms and the right-hand side constitute the Galerkin formulation of the problem. The first series of element-level integrals are the SUPG and PSPG stabilization terms added to the variational formulation. While the SUPG terms stabilize the formulation in the presence of advection operator, the PSPG terms allow one to use any combination of velocity and pressure interpolation, including equal-order interpolation. The second series of element-level integrals are added to the formulation for numerical stability at high Reynolds numbers. For more details on the formulation, definitions of the various coefficients related to the stability terms, and the application to flow past cylinders the reader is referred to the article by Mittal and Kumar [11], Mittal [12], Tezduyar [13] and Tezduyar *et al.* [14]. The element length, utilized in the stabilization coefficients, is equal to the minimum edge length of an element.

4. THE PROBLEM SET-UP

Consider a circular cylinder, of diameter D, placed in a uniform flow of speed U. The free-stream flow is along the x-axis and the cylinder sits at the origin of the coordinate axes. The outer boundary of the computational domain is a square box whose edges are each located at $50D$ from the cylinder centre. The Reynolds number (Re), based on the diameter of the cylinder, free-stream velocity and viscosity of the fluid, for this study varies from 50 to 350.

4.1. The finite element mesh

Figure 1 shows a view of the finite element mesh employed for most of the computations in this paper. It consists of 49 800 quadrilateral elements and 50 315 nodes. At each time step, approximately, 150 000 nonlinear equations are solved via the GMRES technique [15] in conjunction with diagonal preconditioners. In the region close to the cylinder, there are 200 elements in the circumferential direction. The thickness of the the first layer of elements, in the direction normal to the cylinder, is $0.001D$. A time step size of $\Delta t = 0.0625$ is utilized for all the computations.

4.2. Boundary conditions

Uniform flow velocity is prescribed at the upstream boundary and no-slip condition on the velocity is specified on the cylinder wall. At the downstream boundary a Neumann-type boundary condition for the velocity is specified that corresponds to zero viscous vector. On the upper and lower boundaries of the domain the flow is allowed to slip; the component of velocity normal to and the components of stress vector along these boundaries are prescribed

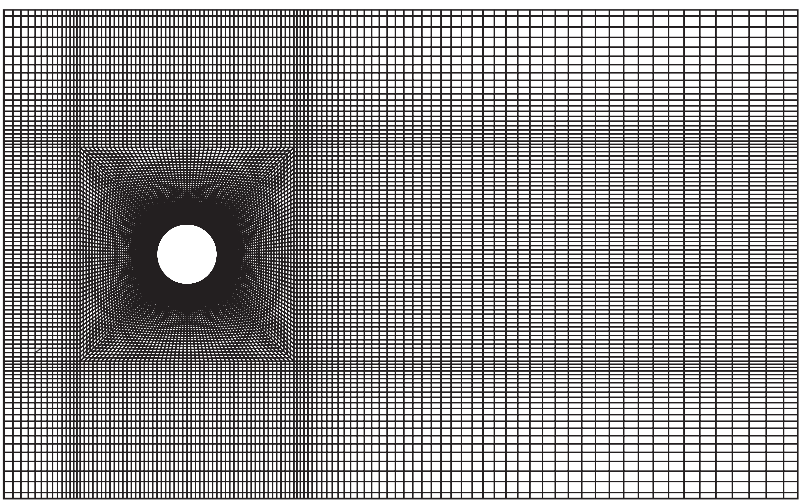

Figure 1. Flow past a cylinder: a close-up view of the finite element mesh with 50 315 nodes and 49 800 elements.

zero value. For the case with no flow across the wake centreline, the vertical component of the velocity at the nodes lying at the wake centreline are assigned a zero value. The flow past half-cylinder is computed by imposing symmetry conditions on the velocity at the wake centreline.

5. RESULTS

5.1. Steady-state solutions

First, steady-state solutions for flow past a cylinder are presented. These solutions are computed by dropping the unsteady terms from the governing equations. Figure 2 shows the

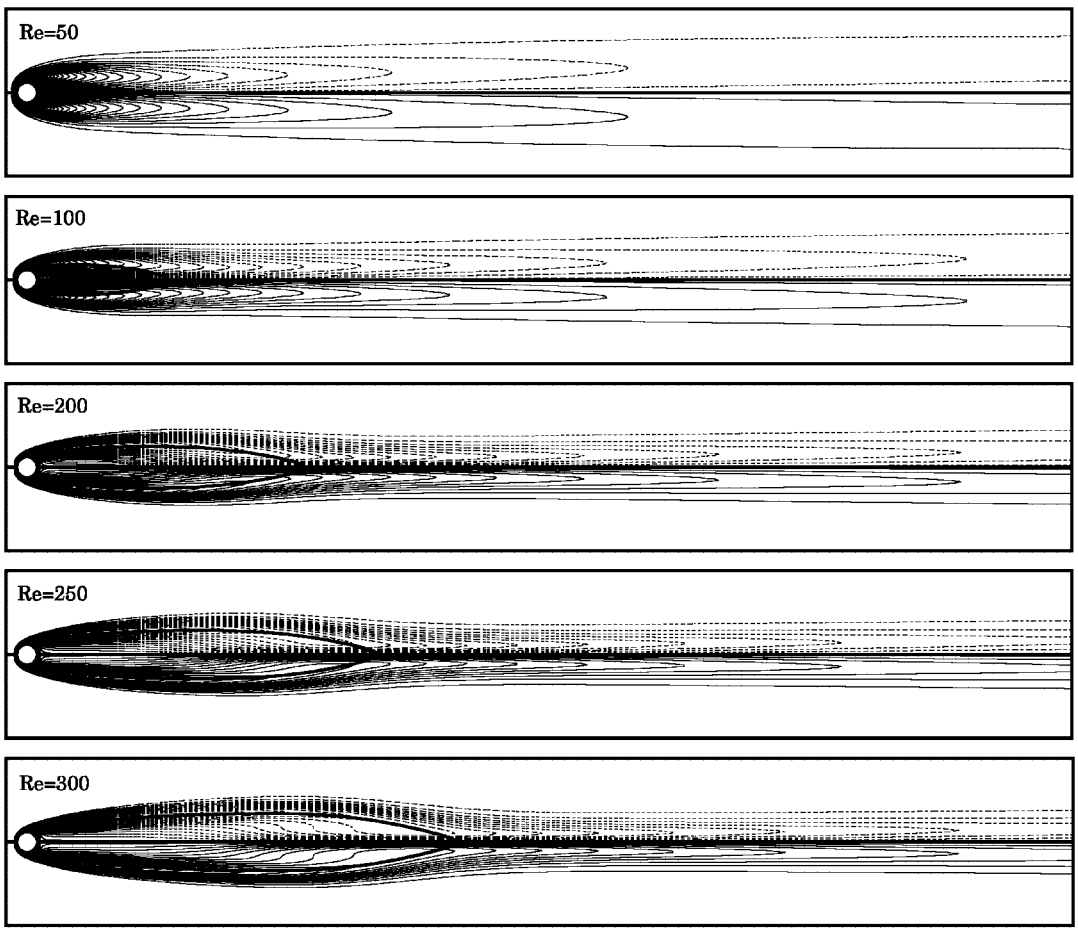

Figure 2. Steady flow past a cylinder at various *Re*: vorticity field. Solid lines indicate counter-clockwise vorticity while the broken lines show clockwise vorticity. The stagnation streamline is shown in thick solid line.

Table I. Steady flow past a cylinder.

Case	Re	$\bar{C}_D$	$\bar{C}_D$ (other studies [16])	L_b/D	C_{p0}	$-C_{pb}$
1	50	1.382	—	3.42	1.134	0.457
2	100	1.065	1.060	6.67	1.075	0.388
3	200	0.837	0.833	13.24	1.044	0.288
4	250	0.779	—	16.78	1.038	0.251
5	300	0.734	0.729	20.49	1.034	0.218

Summary of the various flow parameters for the steady flow past a cylinder at various Reynolds numbers: $\bar{C}_D$, drag coefficient; L_b/D, length of recirculation bubble; C_{p0}, stagnation pressure coefficient; and $-C_{pb}$, base pressure coefficient.

steady-state vorticity fields for the flows at various Re. Also, shown in the same figure, in thick lines, are the stagnation streamlines that represent the recirculation region/wake bubble in the flow at the corresponding Re. Table I lists the various parameters associated with the flows. The flow pictures and the parameters listed in Table I match very well with the results presented by Fornberg [16, 17]. For example, the steady-state drag coefficient from the present computations for $Re = 100$ flow is 1.065 and the length of the wake bubble, measured from the cylinder centre, is $6.67D$. These values, reported by Fornberg [16, 17] are 1.06 and $6.85D$, respectively. It is observed that the recirculation bubble length increases with Re.

The magnitude of the flow speed is shown in Figure 3. Figure 4 shows the velocity profile in the wake of the cylinder at $x/D = 2.5$ and 40 for various Re. The station $x/D = 2.5$ is in the near wake of the flow and highlights the velocity profile in the regions of separated shear layer and recirculation zone. $x/D = 40$ shows the velocity profile beyond the recirculation bubble, in the far wake. From these two figures it can be observed that the thickness of the shear layer separating from cylinder surface decreases with Re. This suggests that the flow at higher Re is more amenable to the instability associated with the shear layer(s). While the steady-state velocity field is symmetric with respect to the centreline, the vorticity field is antisymmetric.

The pressure distribution on the cylinder surface for various Re is shown in Figure 5. The maximum suction on the cylinder surface reduces with increase in Reynolds number. The location of the peak suction moves more towards the lee-ward side of the cylinder with increase in Re. As observed by researchers in the past, the stagnation pressure coefficient at low Re is observed to be larger than 1.0.

5.2. *Unsteady solutions: no condition on wake centreline*

It is well known that the flow past a cylinder becomes unstable at $Re \sim 47$ [1, 18]. In this section, results are presented for the unsteady computations for various Re following an impulsive start. To establish confidence in the finite element formulation, its implementation and the mesh, the results are compared with those available from other studies. Figure 6 shows the vorticity field for the fully developed unsteady flow at various Re. The time instant for which the flow pictures are shown corresponds to the one at which the cylinder experiences peak value of lift force. The characteristic von Karman vortex shedding is observed in all the cases. It is also observed that the longitudinal spacing between the vortices decreases with increase in Re. This spacing is related to the vortex shedding frequency. Table II shows

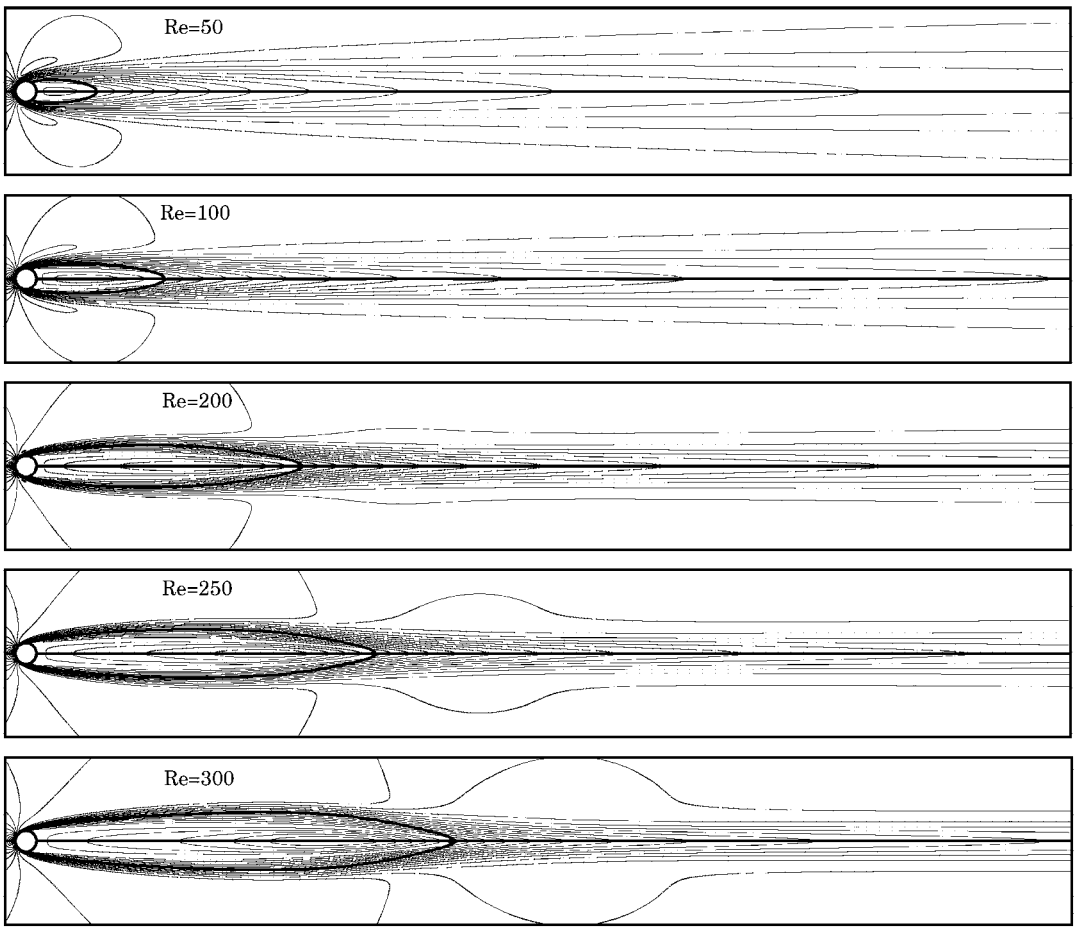

Figure 3. Steady flow past a cylinder at various *Re*: magnitude of the velocity field. The stagnation streamline is shown in thick solid line.

the summary of the aerodynamic coefficients for the flow. The Strouhal number (St), non-dimensional vortex shedding frequency, increases with Re.

These results are in good agreement with those from other research efforts. For example, for the $Re = 100$ flow the Strouhal number (based on the dominant frequency in the variation of the lift coefficient) from the present computations is 0.1644. Williamson [20] measured $St = 0.1648$ for parallel shedding. Kravchenko *et al.* [22] have reported their computed value to be 0.164. They have used a B-Spline method in conjunction with zonal grids. The computations by Persillon and Braza [23] also result in a Strouhal number of 0.164. The rms lift coefficient from the present computations is 0.2256. From the approximate formula suggested by Norberg [24] ($C_{L_{\text{rms}}} = \sqrt{\varepsilon/30 + \varepsilon^2/90}$, $\varepsilon = (Re - 47)/47$), the value is 0.2274. The amplitude of the lift coefficient from the present computations is 0.319. The value reported by Kravchenko *et al.* [22] is 0.314. For the $Re = 200$ flow, the values for the two-dimensional

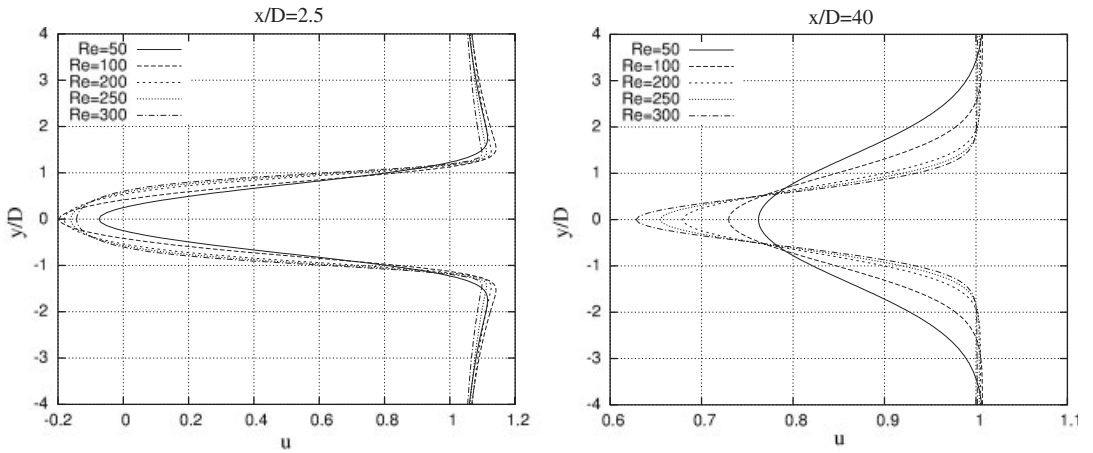

Figure 4. Steady flow past a cylinder at various *Re*: velocity profile in the wake at $x/D = 2.5$ and 40.

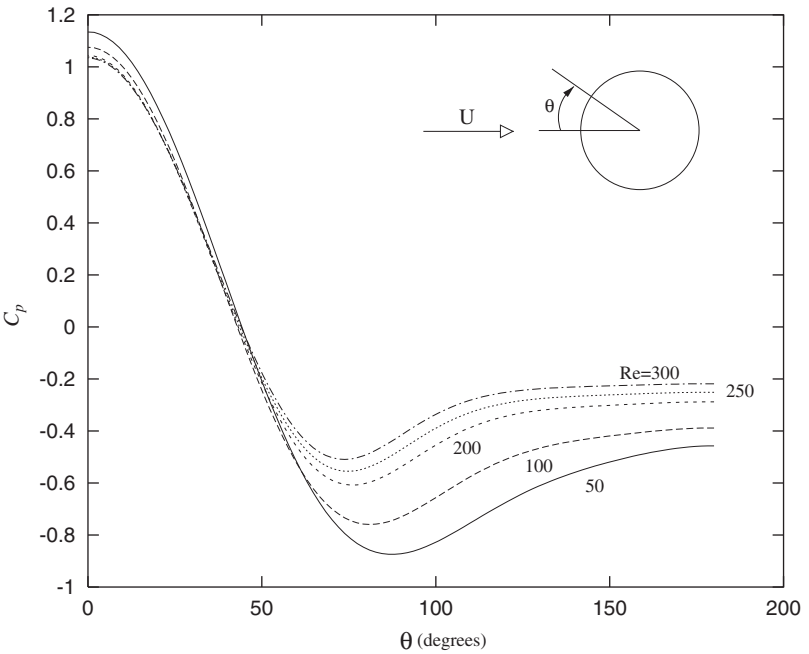

Figure 5. Steady flow past a cylinder at various *Re*: variation of the coefficient of pressure on cylinder surface.

computations reported by Posdziech and Grundmann [25] are 1.3132 for $\bar{C}_D$ and 0.1944 for *St*. The experimentally measured value for *St* is 0.196 [21]. Again, the comparison with the present results is excellent.

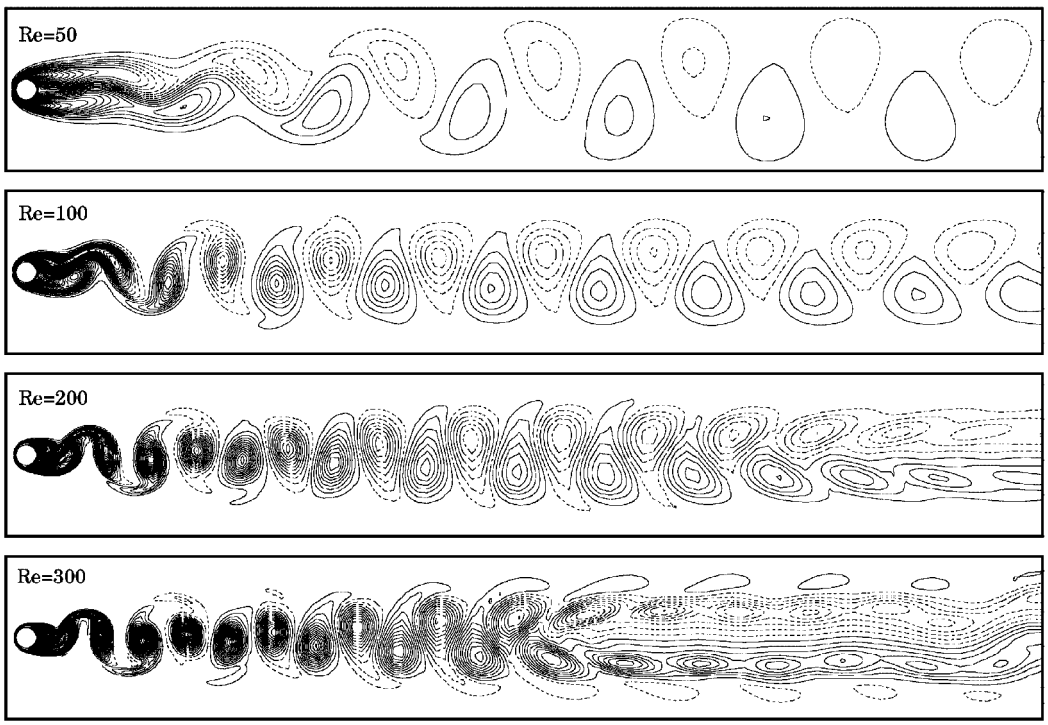

Figure 6. Unsteady flow past a cylinder at various Re: vorticity field for the fully developed unsteady solution at a time instant corresponding to the peak value of lift coefficient. Solid lines indicate counter-clockwise vorticity while the broken lines show clockwise vorticity.

Table II. Unsteady flow past a cylinder at various Re.

Case	Re	$\bar{C}_D$	$(C_D)_{\text{rms}}$	$(C_L)_{\text{rms}}$	St	St (other studies)
1	50	1.416	7.50×10^{-5}	0.035	0.1227	0.1222 [19]
2	100	1.322	6.34×10^{-3}	0.226	0.1644	0.1648 [20]
3	200	1.327	3.09×10^{-2}	0.489	0.1947	0.196 [21]
4	300	1.357	5.63×10^{-2}	0.652	0.2077	—

Summary of the aerodynamic coefficients: $\bar{C}_D$ is the mean drag coefficient, $(C_D)_{\text{rms}}$ and $(C_L)_{\text{rms}}$ are the rms values of the drag and lift coefficients, respectively, and St is the Strouhal number.

The flow past a cylinder is known to become three-dimensional beyond $Re \sim 180$. In such a situation the two-dimensional computations over-predict the Strouhal number and the mean drag coefficient [12, 26]. The three-dimensional computations for the $Re = 300$ flow with slip side walls by Mittal [12], using a very similar finite element formulation as in this work, results in $St = 0.203$. The present two-dimensional computations, as expected, result in a slightly larger

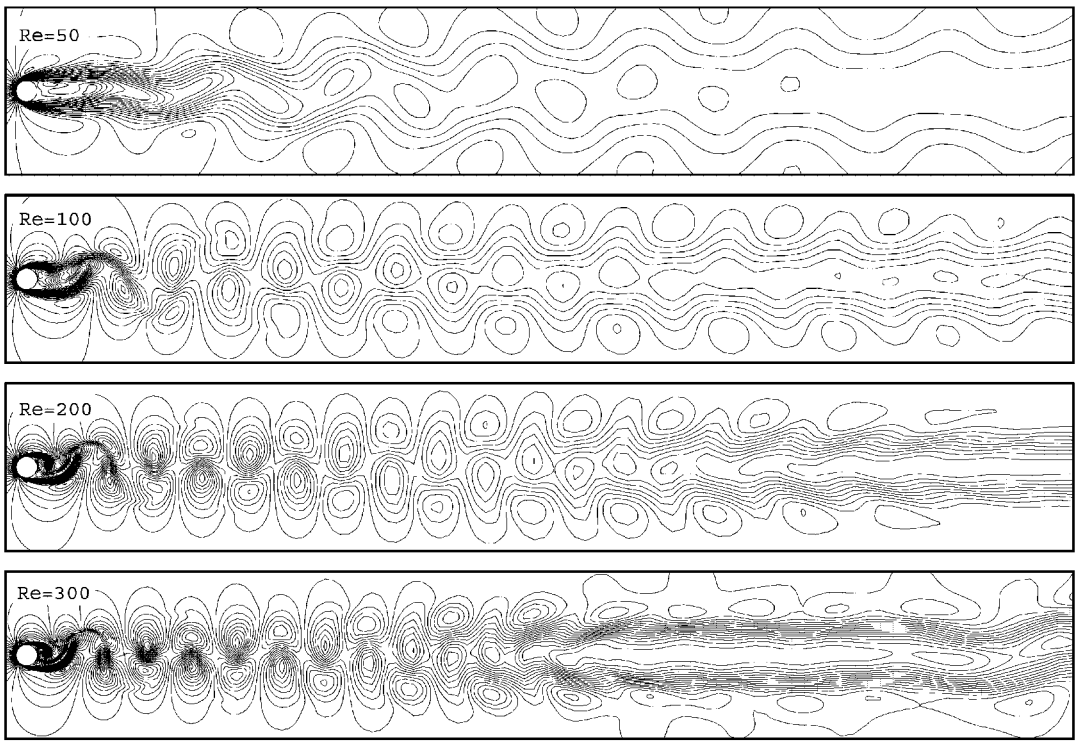

Figure 7. Unsteady flow past a cylinder at various *Re*: magnitude of the velocity field for the fully developed unsteady solution at a time instant corresponding to the peak value of lift coefficient.

value of *St*. Kravchenko *et al.* [22], from their three-dimensional computations, observed $St = 0.203$ and $\bar{C}_D = 1.28$. The corresponding experimental values from Williamson [1] are 0.203 and 1.22.

It is observed from Figures 6 and 7 that for $Re \geqslant 200$ the vortices far downstream in the wake coalesce. The point at which the coalescence begins moves upstream with increase in *Re*. For the $Re = 300$ flow, the far downstream part of the wake exhibits flow structures reminiscent of the secondary instability of the wake [27]. An even larger spatial domain would be required to investigate this instability. This, however, is not the aim of the present study.

5.3. No flow across the wake centreline

It was shown in one of our earlier studies [7] that a 'slip' splitter plate of appropriate length and placed suitably along the wake centreline can suppress the vortex shedding completely for $Re = 100$. The plate allows slip of velocity in the x direction but forces the component of velocity in the y direction to vanish. Our studies show that a slip splitter plate that extends from the rear stagnation point of the cylinder to far downstream, along the wake centreline, suppresses all the instabilities for $Re \leqslant 300$ (and perhaps, for larger *Re* which we have not investigated). To excite the shear layer instability, we present results for computations where

the entire wake centreline downstream of the cylinder is forced to be streamline: no flow normal to this line is allowed. It is hoped that such an arrangement will weaken/suppress the vortex shedding mode so that the shear layer instability is exposed.

Computations are carried out for $Re = 50$, 100, 200, 250, 300 and 350 with the initial conditions corresponding to an impulsive start. It was observed that for $Re = 250$ and below, no instabilities are observed and the flow remains steady. However, for the $Re = 300$ flow, an interesting instability is observed.

Figure 8 shows the time histories and their power spectra of the vertical component of velocity at a point located at $(10.06D, 0.63D)$. The data for both the computations, with and without the no-normal-flow across the wake centreline, is shown. For the case without any condition on the wake centreline the time variation associated with the data is due to the von Karman vortex shedding. The power spectra shows the peak for the vortex shedding frequency, f_K, and its harmonics. For the case with the no-normal-flow across the wake centreline, the signal consists of an almost time periodic variation of a very low frequency along with intermittent oscillations corresponding to f_{SL} and its super harmonics. Here, f_{SL} denotes the shear layer frequency. We observe that f_{SL} is significantly smaller than f_K. Time histories of the velocity components and their power spectra at points located elsewhere in the wake, for example at $(2D, 1D)$, show similar behaviour.

Figure 9 shows the vorticity field at various instants during one cycle of variation of this signal. Also shown in the right column of the figure is the disturbance to the vorticity field with respect to the steady-state solution for the $Re = 300$ flow. It can be observed, from the figure, that the disturbance first appears in the far downstream part of the wake (frames c and d of Figure 9) and than propagates upstream. From this figure it appears that the instability begins as a wake instability leading to the vortex shedding. As the disturbance moves upstream to the recirculation zone near the cylinder, it excites the instability of the separated shear layer. This instability is qualitatively different from the von Karman vortex shedding shown in Figure 6. It is intermittent as was also observed by researchers earlier [3, 4] and its frequency f_{SL} is significantly different from the vortex shedding frequency, f_K, that is observed for the flow past a cylinder with no constraint along the centreline. Also, the magnitude of unsteadiness in the shear layer instability is significantly smaller than in the von Karman vortex shedding. This can be observed from the time histories of the cross-flow component of velocity at a point shown in Figure 8. The same observation can also be made from the comparison between the unsteady component of the drag coefficient obtained for the cases with and without the no-normal-flow condition across the wake centreline as shown in Figure 10. This suggests that at $Re = 300$ the shear layer instability is much weaker compared to the primary instability of the wake. In addition, in a real situation the flow is contaminated with three-dimensional instabilities. Perhaps, that is why one does not observe the shear layer instability during most experiments. So far, only the experiments conducted by Gerrard [3] have reported the presence of shear layer vortices at low Re. The present computations show that it is possible to excite the shear layer instability even for $Re = 300$. It can be observed if the other instabilities that are much stronger, for example, the primary instability are suppressed or weakened.

Our preliminary results from the linear stability analysis also support the results from these two-dimensional direct numerical simulations. The steady-state solution for $Re = 250$ is found stable, while that at $Re = 300$ is unstable. The eigenmode corresponding to the rightmost eigenvalue (with largest real part) appears very similar to the flow pictures in Figure 9.

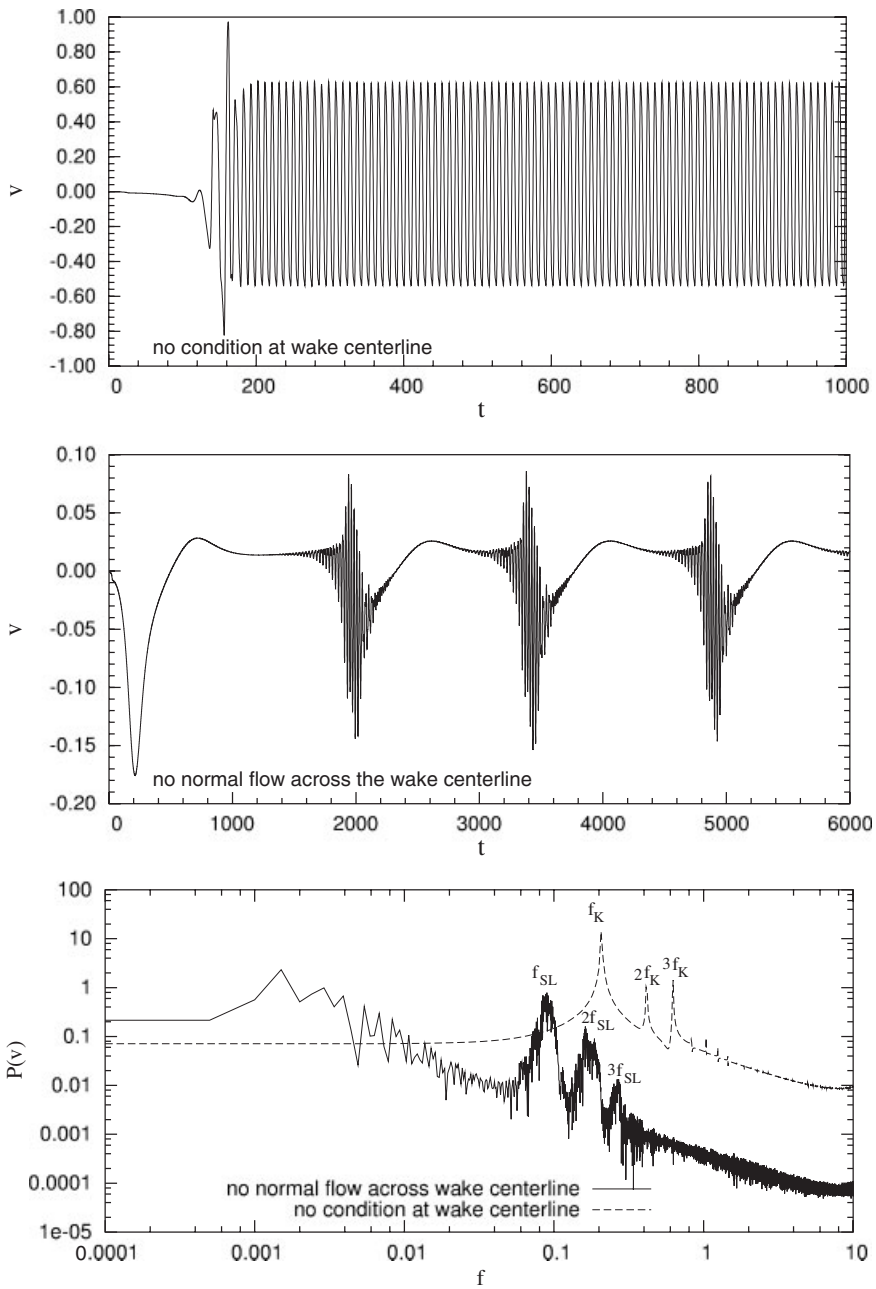

Figure 8. $Re = 300$ flow past a cylinder with and without the no-flow condition across the wake centreline: time histories and their power spectra of the vertical component of velocity at a point located at $(10.06D, 0.63D)$. The frequency f has been non-dimensionalized using the diameter of the cylinder and the free-stream speed.

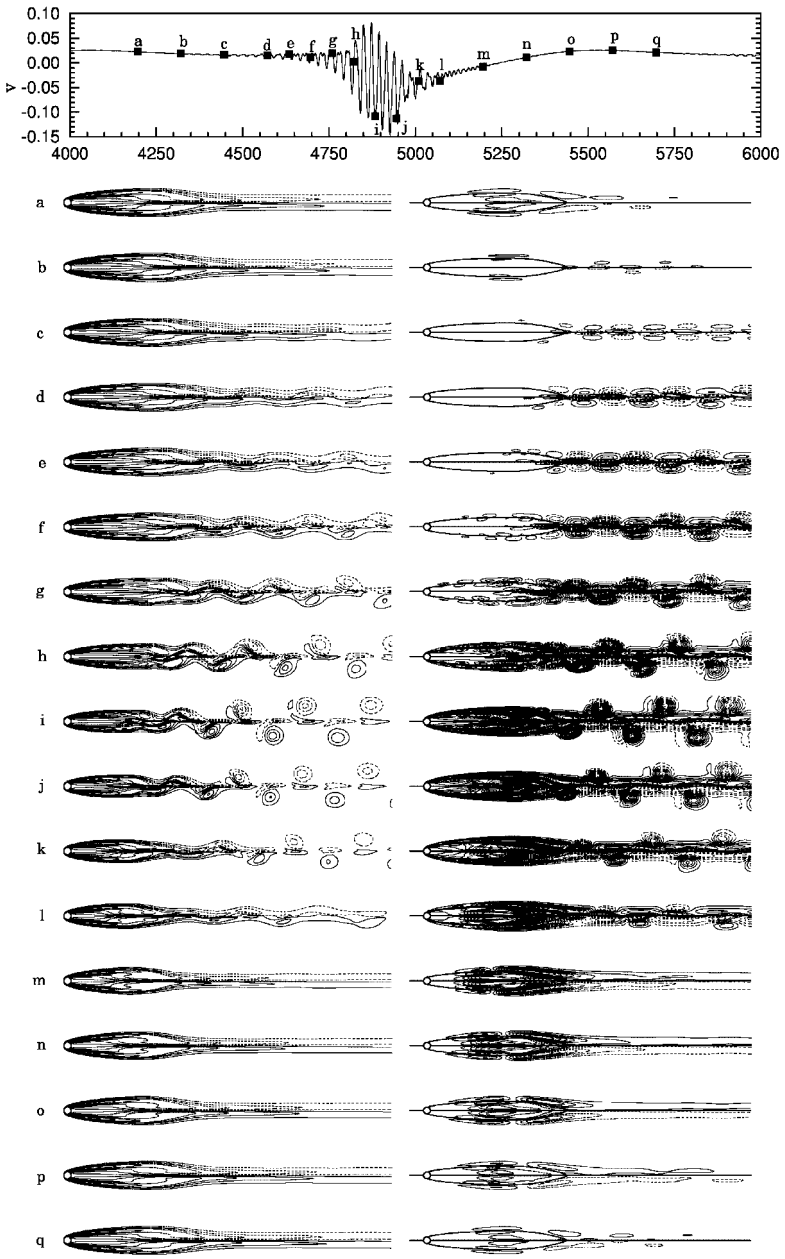

Figure 9. $Re = 300$ flow past a cylinder with the no-flow condition across the wake centreline: vorticity field (left) and its fluctuating part (right) at various instants during one cycle of the unsteady solution. Also shown is the time history of the vertical component of velocity at a point $(10.06D,\ 0.63D)$ with respect to the centre of the cylinder. The stagnation streamline for the steady solution is shown in a thicker solid line. Solid lines indicate counter-clockwise vorticity while the broken lines show clockwise vorticity.

Presently, we are trying to locate the critical Re at which the shear layer instability sets in. These results will be reported in a later article.

Figure 12 shows the time histories of the vertical component of velocity at a point located at $(10.06D, 0.63D)$ and their power spectra for $Re = 350$. The results are very similar to those at $Re = 300$. Prasad and Williamson [4] found that the normalized shear layer frequency (f_{SL}/f_K), equivalent to the non-dimensional shedding frequency of the secondary vortices as used by Wei and Smith [28], follows the $Re^{0.67}$ power law. In fact, they [4] plotted not only their own data but also that from all the previous investigators and found that the $Re^{0.67}$ power law gives a much closer fit than the $Re^{0.5}$ law proposed earlier, from approximate analysis. In that sense, the $Re^{0.67}$ power law represents almost all the experimental data that exists. In the present work, we have results from two sets of Re: $Re = 300$ and 350. We proceed to check if the present data follows the $Re^{0.67}$ power law. To this extent, it is found that the ratio of values of f_{SL}/f_K at $Re = 350$ and 300 is 1.106. This is in good agreement with the value from the power law: $((350/300)^{0.67} = 1.109)$.

5.4. Flow past half a cylinder: is the separated shear layer intrinsically unstable?

In light of the instability of the shear layer, observed for $Re = 300$, a question that deserves attention is whether the separated shear layer in intrinsically unstable or that the shear layer instability observed in the previous section has been excited by the instability of the wake. To address this issue flow past half a cylinder (the upper part) is computed.

The computational domain and the finite element mesh are exactly one half of the ones used for the complete cylinder. On the lower boundary of the cylinder, along the cylinder centreline, the component of velocity normal to it is prescribed a zero value. In addition, the component of stress vector along this boundary is assigned a zero value. All the other boundary conditions are same as for the flow past a full cylinder.

Flow past half a cylinder was computed for $Re = 100$, 200 and 300 following an impulsive start. In all the cases, the flow achieved a steady state. The steady-state lift and drag coefficients are listed in Table III. Figure 10 shows the time histories of the drag coefficient for the complete and half-cylinder for the $Re = 300$ flow. In this figure, the drag coefficient for the half-cylinder, has been multiplied by two to aid comparison with the results for the full cylinder. The vorticity field for the fully developed solution for various Re is shown in Figure 11. The solutions are virtually identical to the upper half of the solutions obtained with the steady-state computations for the full cylinder. This computation demonstrates that the separated shear layer is intrinsically stable for the flow at $Re = 300$. However, it can be excited by other disturbances such as the primary wake instability. The computations provide a possible explanation for the shear layer instability seen by Gerrard [3] for low Re flows. As has been reported by other investigators in the past, at a higher Re, the separated shear layer becomes unstable on its own. Flow past half a cylinder can be studied to find the critical Re for the onset of shear layer instability. This is currently under investigation.

5.5. Flow past half a cylinder: excitation of the separated shear layer by a secondary cylinder

Having confirmed that the flow past half a cylinder is globally stable at $Re = 300$, we investigate its receptivity to external excitation. A secondary cylinder of one-fifth the diameter of

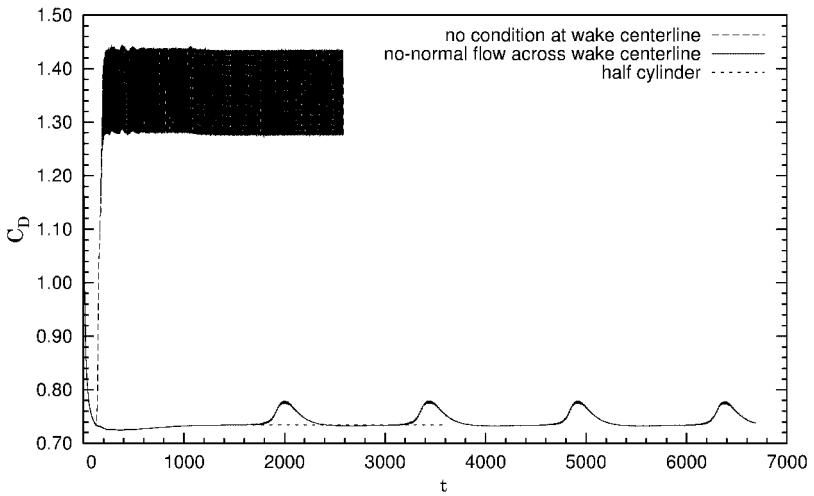

Figure 10. $Re = 300$ flow past a cylinder with and without the no-flow condition across the wake centreline: time histories of the drag coefficient. Also shown is the drag coefficient for the half-cylinder that is multiplied by two.

Table III. Flow past half a cylinder at various *Re*: value of the drag and lift coefficient for the fully developed flow.

Case	*Re*	C_D	C_L
1	100	0.5335	0.5373
2	200	0.4186	0.3794
3	300	0.3671	0.2826

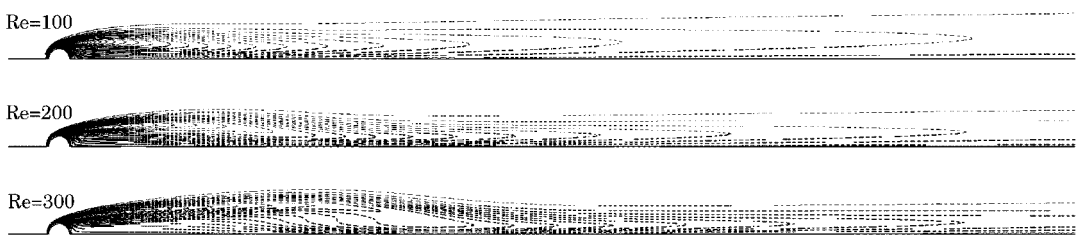

Figure 11. Flow past a half-cylinder at various *Re*: vorticity field for the fully developed solution. Solid lines indicate counter-clockwise vorticity while the broken lines show clockwise vorticity.

the main cylinder is placed at $(-1.0D, 2.5D)$ with respect to the centre of the half-cylinder. Based on its diameter and the free-stream speed the Reynolds number for the smaller cylinder is 60. This is large enough to result in vortex shedding. We investigate the possibility that the vortex shedding from the smaller cylinder might excite the instability of the separated shear layer from the half-cylinder. The finite element mesh consists of 97 474 nodes and 194 056 triangular elements (Figure 12).

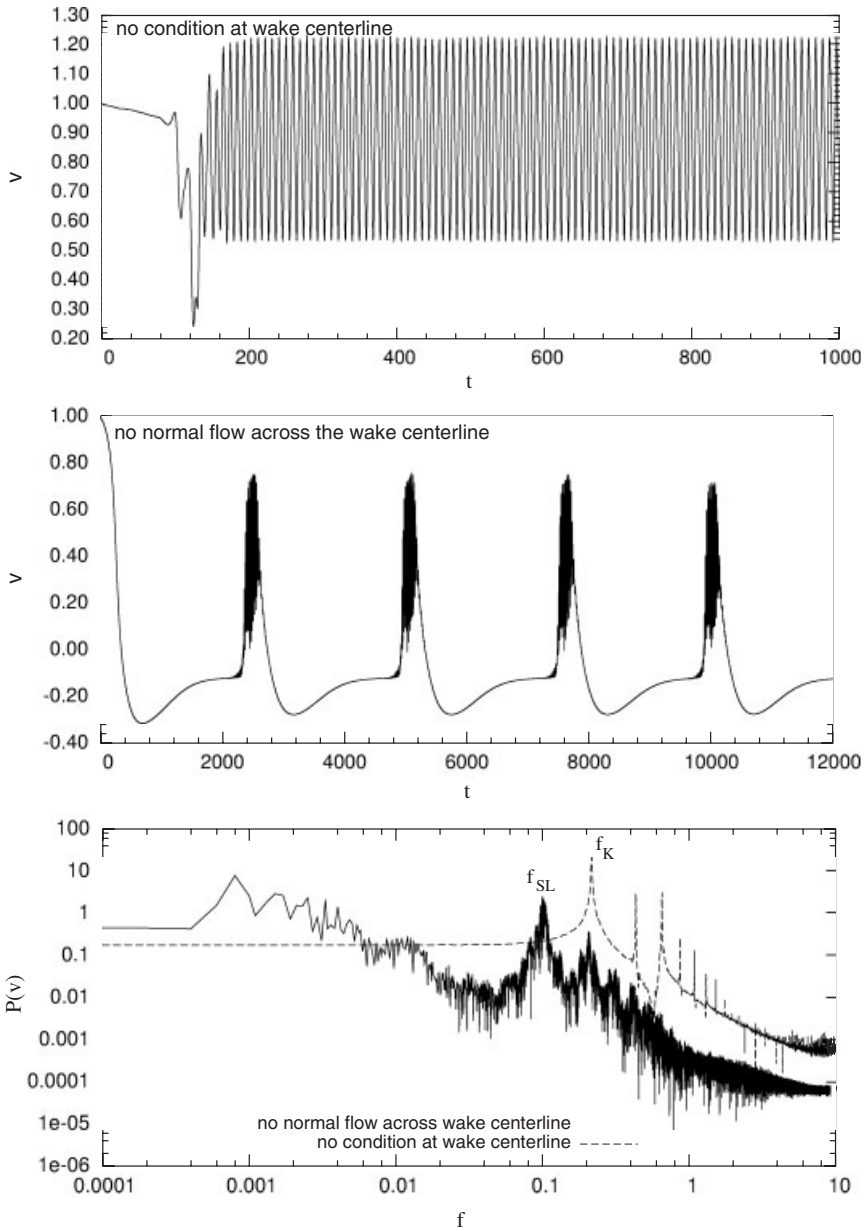

Figure 12. $Re = 350$ flow past a cylinder with and without the no-flow condition across the wake centreline: time histories and their power spectra of the vertical component of velocity at a point located at $(10.06D, 0.63D)$. The frequency f has been non-dimensionalized using the diameter of the cylinder and the free-stream speed.

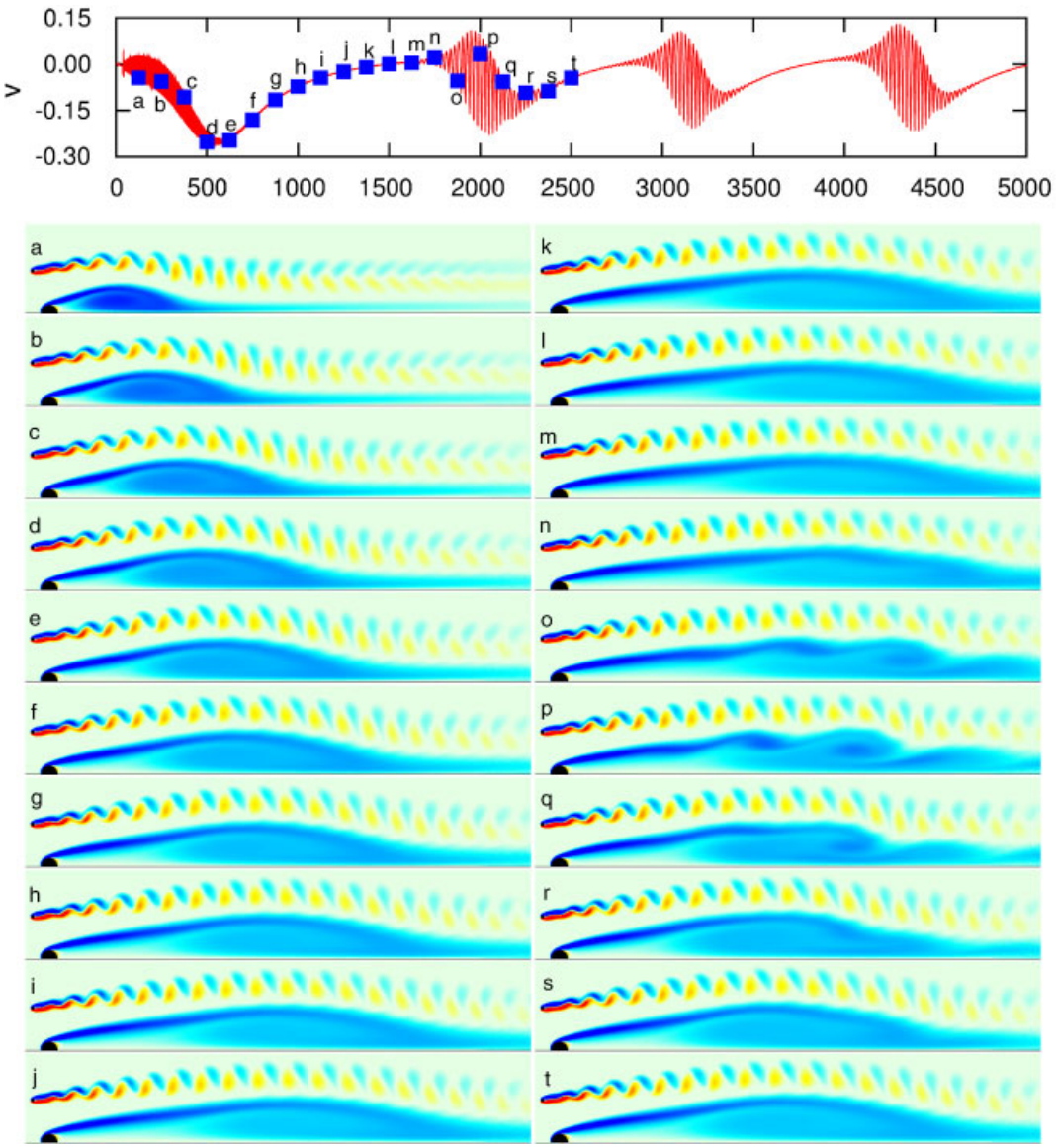

Figure 13. $Re = 300$ flow past half a cylinder in the presence of a smaller secondary cylinder of one-fifth the diameter: time history of the vertical component of velocity at $(15D, 2D)$ and vorticity field at various time instants. Red colour indicates counter-clockwise vorticity while the blue colour shows clockwise vorticity.

Figure 13 shows the time history of the vertical component of velocity at a point whose coordinates, with respect to the centre of the half-cylinder, are $(15D, 2D)$. The instantaneous vorticity field at certain time instants is also shown in the same figure. As expected, Karman vortex street is established behind the smaller cylinder. A recirculation bubble forms

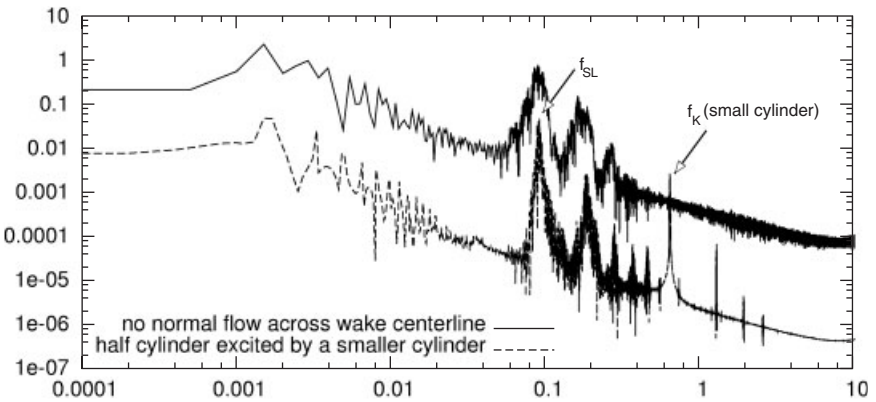

Figure 14. Power spectra of the vertical component of velocity at a point in the $Re = 300$ flow past a cylinder from two simulations: no-flow condition across the wake centreline and half-cylinder wake excited by a smaller secondary cylinder.

in the wake of the half-cylinder and increases in size with time. The growth of the bubble can be observed in frames a–g of Figure 13. As a result of this bubble, the vortex street from the smaller cylinder is slightly displaced. At $t \sim 1750$ (frame n of Figure 13), slight oscillations in the downstream part of the recirculation bubble can be observed. Subsequently, these oscillations grow and result in the shear layer vortices (frames o–q of Figure 13). This instability resembles the Kelvin Helmholtz instability of the shear layer. After some time the disturbances are swept off and the flow achieves a quiet state. However, the instability returns at $t \sim 2750$ and the instability of the separated shear layer is observed, yet again. As can be seen from the time history of the velocity, shown in the top row of the same figure, this instability establishes itself as a periodic, intermittent phenomenon.

It is seen from Figure 13 that the transition point of shear layer, beyond which it is unstable, is quite far from the cylinder. This is in line with the observations by Singh and Mittal [29] who investigated the possible relationship between the drag crisis (sudden loss of drag at $Re \sim 2 \times 10^5$) and the instability of the separated shear layer via two-dimensional simulations. They observed that as Re is increased the transition point of shear layer, beyond which it is unstable, moves upstream.

The instability observed in this simulation and the one with a full cylinder with the condition of the no-normal-flow across the wake centreline seem very similar: both show a periodic and intermittent behaviour. Shown in Figure 14 are the frequency spectra of the vertical component of the velocity from the two simulations. While the result for the simulation with the no-normal-flow across the wake centreline is for a probe located at $(10.06D, 0.63D)$, the probe for the half-cylinder is located at $(1.5D, 0.51D)$. In both the cases, the peak corresponding to f_{SL} is observed at the same frequency. The power spectra from the velocity recorded by probes at other locations, for both the simulations, give very similar results. This adds further confidence in the present results.

Also observed in the spectrum for the half-cylinder case is a peak corresponding to the vortex shedding frequency for the smaller secondary cylinder ($f_K \sim 0.638$). Based on the di-

ameter of the smaller cylinder, this value of f_K corresponds to $St = f_K/5 \sim 0.128$ which seems quite reasonable for $Re = 60$ flow past a cylinder (please see Table II). At higher Re, the frequency of the formation of shear layer vortices is higher than the primary vortex shedding frequency [29]. It is seen here, that for low Re, f_{SL} is significantly smaller than the primary vortex shedding frequency. These simulations establish that even though the separated shear layer from the cylinder is intrinsically stable at $Re = 300$, it can be excited via external disturbance(s). This points to the shear layer being convectively unstable as opposed to the wake which is absolutely unstable. More work, to address this aspect, is currently in progress.

6. CONCLUDING REMARKS

A stabilized finite element method has been utilized to compute flow past a cylinder, in two dimensions, at low Reynolds numbers ($50 \leqslant Re \leqslant 350$). Steady and unsteady flows past a circular cylinder have been computed and compared with the available experimental and computational results in the literature. Good agreement has been observed. It is observed that for $Re \geqslant 200$ the vortices far downstream in the wake coalesce. At $Re = 300$, downstream of the coalescence, an interesting vortex structure, resembling the secondary vortex shedding, is observed. This warrants further investigation with a larger computational domain.

A numerical experiment has been conducted wherein the wake centreline is forced to be a streamline. The initial conditions correspond to an impulsive start. Forcing the no-normal-flow across the centreline suppresses the primary instability of the wake, that is responsible for the von Karman vortex shedding, for $Re < 250$. At $Re = 300$, instability in the flow sets in. Along with the wake instability, shear layer instability is observed for the $Re = 300$ flow. The fluctuations due to the instability are intermittent in nature and much weaker than those for the von Karman vortex shedding for flow past a cylinder without the imposition of the no-normal-flow across the wake centreline. The observation of shear layer instability at such a low Re has been made possible by the weakening of the, more dominating, primary instability of the wake. Similar instability is observed for the $Re = 350$ flow, as well. It is found that the normalized shear layer frequency scales with the $Re^{0.67}$ power law, even at these low Re.

Computations have also been carried out for flow past half a cylinder with symmetry boundary conditions on the velocity field at the centreline. This numerical experiment is useful in assessing the stability of an isolated shear layer as opposed to the pair of shear layers that exist in the full cylinder. It is found that that the $Re = 300$ flow past half a cylinder is stable. However, when a secondary cylinder of one-fifth the diameter of the half-cylinder is placed close to it, the vortex shedding from the smaller cylinder excites the instability of the separated shear layer of the half-cylinder. The shear layer frequency from this simulation matches the one for full cylinder with no flow across the wake centreline. The present investigation suggests that although the shear layer at $Re = 300$ is intrinsically stable, it is possible to excite it by some other disturbances.

ACKNOWLEDGEMENTS

The Department of Science and Technology India, is gratefully acknowledged for providing partial support to this work.

REFERENCES

1. Williamson CHK. Vortex dynamics in the cylinder wake. *Annual Review of Fluid Mechanics* 1996; **28**: 477–539.
2. Roshko A. Perspectives on bluff body aerodynamics. *Journal of Wind Engineering and Industrial Aerodynamics* 1993; **49**:79–100.
3. Gerrard JH. The wakes of cylindrical bluff bodies at low Reynolds number. *Philosophical Transactions of the Royal Society of London Series A* 1978; **288**:351–382.
4. Prasad A, Williamson CHK. The instability of the shear layer separating from a bluff body. *Journal of Fluid Mechanics* 1997; **333**:375–402.
5. Unal MF, Rockwell D. On the vortex formation from a cylinder Part 1. The initial instability. *Journal of Fluid Mechanics* 1988; **190**:491–512.
6. Bloor MS. The transition to turbulence in the wake of a circular cylinder. *Journal of Fluid Mechanics* 1964; **19**:290.
7. Mittal S. Effect of a 'slip' splitter plate on vortex shedding from a cylinder. *Physics of Fluids* 2003; **15**: 817–820.
8. Braza M, Chassaing P, Ha Minh H. Prediction of large-scale transition features in the wake of a circular cylinder. *Physics of Fluids A* 1990; **2**:1461–1471.
9. Roshko A. On the drag and shedding frequency of two-dimensional bluff bodies. *Technical Report TN 3169*, NACA, 1954.
10. Unal MF, Rockwell D. On the vortex formation from a cylinder Part 2. Control by splitter-plate interference. *Journal of Fluid Mechanics* 1988; **190**:513–529.
11. Mittal S, Kumar B. Flow past a rotating cylinder. *Journal of Fluid Mechanics* 2003; **476**:303–334.
12. Mittal S. Computation of 3D flows past circular cylinders of low aspect ratio. *Physics of Fluids* 2001; **13**: 177–191.
13. Tezduyar TE. Finite element methods for fluid dynamics with moving boundaries and interfaces. *Encyclopedia of Computational Mechanics*. Wiley: New York, 2004.
14. Tezduyar TE, Mittal S, Ray SE, Shih R. Incompressible flow computations with stabilized bilinear and linear equal-order-interpolation velocity-pressure elements. *Computer Methods in Applied Mechanics and Engineering* 1992; **95**:221–242.
15. Saad Y, Schultz M. GMRES: a generalized minimal residual algorithm for solving nonsymmetric linear systems. *SIAM Journal on Scientific and Statistical Computing* 1986; **7**:856–869.
16. Fornberg B. Steady viscous flow past a circular cylinder up to Reynolds number 600. *Journal of Computational Physics* 1985; **98**:297–320.
17. Fornberg B. A numerical study of steady viscous flow past a circular cylinder. *Journal of Fluid Mechanics* 1980; **98**:819–855.
18. Norberg C. An experimental investigation of the flow around a circular cylinder: influence of aspect ratio. *Journal of Fluid Mechanics* 1994; **258**:287–316.
19. Norberg C. Fluctuating lift on a circular cylinder: review and new measurements. *Journal of Fluids and Structures* 2003; **17**:57–96.
20. Williamson CHK. Oblique and parallel modes of vortex shedding in the wake of a circular cylinder at low Reynolds numbers. *Journal of Fluid Mechanics* 1989; **206**:579–627.
21. Miller GD, Williamson CHK. Control of three-dimensional phase dynamics in a cylinder wake. *Experiments in Fluids* 1994; **18**:26–35.
22. Kravchenko AG, Moin P, Shariff K. B-spline method and zonal grids for simulations of complex turbulent flows. *Journal of Computational Physics* 1999; **151**:757–789.
23. Persillon H, Braza M. Physical analysis of the transition to turbulence in the wake of a circular cylinder by three-dimensional Navier–Stokes simulation. *Journal of Fluid Mechanics* 1998; **365**:23–88.
24. Norberg C. Flow around a circular cylinder: aspects of fluctuating lift. *Journal of Fluids and Structures* 2001; **15**:459–469.
25. Posdziech O, Grundmann R. Numerical simulation of the flow around an infinitely long circular cylinder in the transition regime. *Theoretical and Computational Fluid Mechanics* 2001; **15**:121–141.
26. Mittal R, Balachander S. Effect of three-dimensionality on the lift and drag of nominally two-dimensional cylinders. *Physics of Fluids* 1995; **7**:1841–1865.
27. Cimbala JM, Gharib HM, Roshko A. Large structure in the far wakes of two-dimensional bluff bodies. *Journal of Fluid Mechanics* 1988; **190**:265–298.
28. Wei T, Smith CR. Secondary vortices in the circular cylinders. *Journal of Fluid Mechanics* 1986; **169**:513–533.
29. Singh SP, Mittal S. Flow past a cylinder: shear layer instability and drag crisis. *International Journal for Numerical Methods in Fluids* 2005; **47**:75–98.

